ADVANCED MATERIALS
www.advmat.de

Parallel Signal Processing of a Wireless Pressure-Sensing Platform Combined with Machine-Learning-Based Cognition, Inspired by the Human Somatosensory System

Gun-Hee Lee, Jin-Kwan Park, Junyoung Byun, Jun Chang Yang, Se Young Kwon, Chobi Kim, Chorom Jang, Joo Yong Sim, Jong-Gwan Yook,* and Steve Park**

Inspired by the human somatosensory system, pressure applied to multiple pressure sensors is received in parallel and combined into a representative signal pattern, which is subsequently processed using machine learning. The pressure signals are combined using a wireless system, where each sensor is assigned a specific resonant frequency on the reflection coefficient (S_{11}) spectrum, and the applied pressure changes the magnitude of the S_{11} pole with minimal frequency shift. This allows the differentiation and identification of the pressure applied to each sensor. The pressure sensor consists of polypyrrole-coated microstructured poly(dimethylsiloxane) placed on top of electrodes, operating as a capacitive sensor. The high dielectric constant of polypyrrole enables relatively high pressure-sensing performance. The coils are vertically stacked to enable the reader to receive the signals from all of the sensors simultaneously at a single location, analogous to the junction between neighboring primary neurons to a secondary neuron. Here, the stacking order is important to minimize the interference between the coils. Furthermore, convolutional neural network (CNN)-based machine learning is utilized to predict the applied pressure of each sensor from unforeseen S_{11} spectra. With increasing training, the prediction accuracy improves (with mean squared error of 0.12), analogous to humans' cognitive learning ability.

Electronic skin has been a rapidly advancing field of research over the past several decades. Electronic skin are devices that mimic the tactile sensing properties of human skin, which can be utilized in applications like wearable electronics, robotics, and prosthetics.[1–5] Thus far, there have been numerous reports on different types and designs of tactile sensing (e.g., pressure and strain) electronic skin devices, which showed continuously improving performance over the years.[6–10] However, tactile sensing technology alone is insufficient to enable the aforementioned applications, where the processing of acquired signal is also of critical importance.[1–3,11] In fact, only when tactile sensing technology is combined with the correspondingly fitting signal processing technology, will various devices be able to perceive and interact with the environment, and hence be able to "feel like a human."[5] In this regard, one could learn and gain inspiration from the human somatosensory system, which is a system of receptors, sensory neurons, and synaptic pathways, through which our body receives and processes tactile information.[12–17] Our somatosensory system has the following interesting features to consider in terms of tactile signal processing (**Figure 1**a). First, the tactile inputs from stimulated receptive fields are simultaneously received and transmitted via primary sensory neurons. Second, at the spinal cord or medulla, the neighboring primary sensory neurons are grouped such that the signals are combined and transmitted as a single output signal to the secondary neuron. Interestingly, the combined signal has the necessary information encoded, such that we are able to differentiate the location and type of stimuli. The secondary neurons carry the signal to

G.-H. Lee, J. C. Yang, S. Y. Kwon, C. Kim, Prof. S. Park
Department of Materials Science and Engineering
Korea Advanced Institute of Science and Technology (KAIST)
Daejeon 34141, Republic of Korea
E-mail: stevepark@kaist.ac.kr

J.-K. Park, C. Jang, Prof. J.-G. Yook
School of Electrical and Electronic Engineering
Yonsei University
Seoul 03722, Republic of Korea
E-mail: jgyook@yonsei.ac.kr

J. Byun
School of Electrical Engineering
Korea Advanced Institute of Science and Technology (KAIST)
Daejeon 34141, Republic of Korea

Dr. J. Y. Sim
Bio-Medical IT Convergence Research Department
Electronics and Telecommunications Research Institute (ETRI)
Daejeon 34129, Republic of Korea
E-mail: jsim@etri.re.kr

The ORCID identification number(s) for the author(s) of this article can be found under https://doi.org/10.1002/adma.201906269.

DOI: 10.1002/adma.201906269

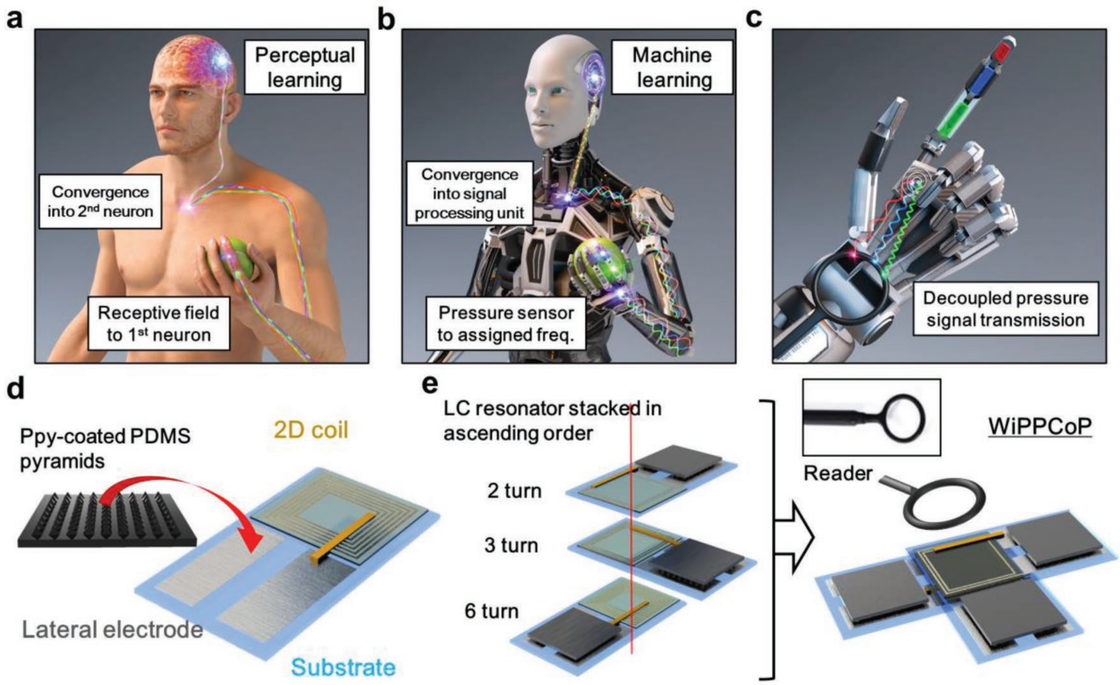

Figure 1. Overall concept of WiPPCoP. a) Illustration of the human somatosensory system. b) Illustration of WiPPCoP on a robotic system. c) Illustration of WiPPCoP on a robotic hand where tactile signal is received simultaneously, each with a specific frequency. d) Schematic depiction of a closed LC resonator on the right, which consists of a 2D coil and lateral electrodes. The left drawing is a depiction of a PDMS substrate that was microstructured with pyramids and coated with polypyrrole; this substrate was placed on top of the lateral electrodes with the pyramids facing down to form the LC pressure sensor. e) Assembling of multiple LC pressure sensors by vertically stacking the 2D coils in ascending order, with the coils with smaller number of turns placed closer to the reader.

a thalamus and connections are made with tertiary neurons via synapses. Finally, the tertiary neurons form a neural network with the neurons in the somatosensory cortex, which is where the processing of tactile information takes place, through which we are able to perceive and learn.[18–25]

In recent years, researchers have begun to mimic the human somatosensory system, where tactile sensors were combined with artificial synaptic devices, by which multiple tactile signals were combined and processed simultaneously.[16,17,26] For instance, Lee et al. made a multi-device system that can convert incoming pressure signals into electrical pulses using ring oscillators, which was then processed by synaptic devices.[16] This system has shown the capability to process multiple pressure signals using a synaptic device. However, it is not possible to ascertain which pressure sensor a given signal is coming from; hence, additional synaptic devices are needed. In another report, two pressure sensors were connected to a single synaptic device where the signals from both pressure sensors were processed simultaneously, and through learning, recognition error was progressively reduced.[17] However, as pressure sensors connected to a synaptic device increase, it will become increasingly complex to differentiate the pressure levels of each sensor. In summary, the sensor-synaptic device systems are currently limited in processing multiple tactile signals, as information is lost during processing. Furthermore, in these systems, complexity in wiring is an unavoidable issue with an increasing number of sensors, which can hinder their practical applicability.

In this work, we introduce WiPPCoP (wireless parallel pressure cognition platform), which possesses the aforementioned key features of the somatosensory system (Figure 1b). WiPPCoP can wirelessly receive pressure information from multiple sensors simultaneously (i.e., in parallel) at a single location using vertically stacked 2D coil architecture and combine the signals into one representative signal pattern (Figure 1c), resembling the connection between the multiple primary neurons to a secondary neuron.[18] WiPPCoP was designed such that each sensor has a specific resonant frequency pole in the S_{11} (reflection coefficient) versus frequency plot (i.e., S_{11} spectrum) on the network analyzer, and the variation in pressure changes the magnitude of the poles with minimal shifting of the resonant frequencies. Such a property allows the assignment of a frequency to each sensor, through which the signal from each sensor can be identified. This is on the contrary to other wireless pressure sensors, where frequency shifting of the poles was used to detect pressure changes.[27–29] Furthermore, since the signal is transmitted wirelessly, off-chip wiring is unnecessary. As a means to generate a cognitive system that mimics the neural network in the somatosensory cortex, using convolutional neural network, our system has been taught to predict the pressure levels of each sensor, given an unforeseen S_{11} spectrum as an input. With increasing training, the accuracy of the predicted output pressure values progressively increased, validating the legitimacy of our machine-learning algorithm. Our system brings forth a new perspective on utilizing wireless system combined

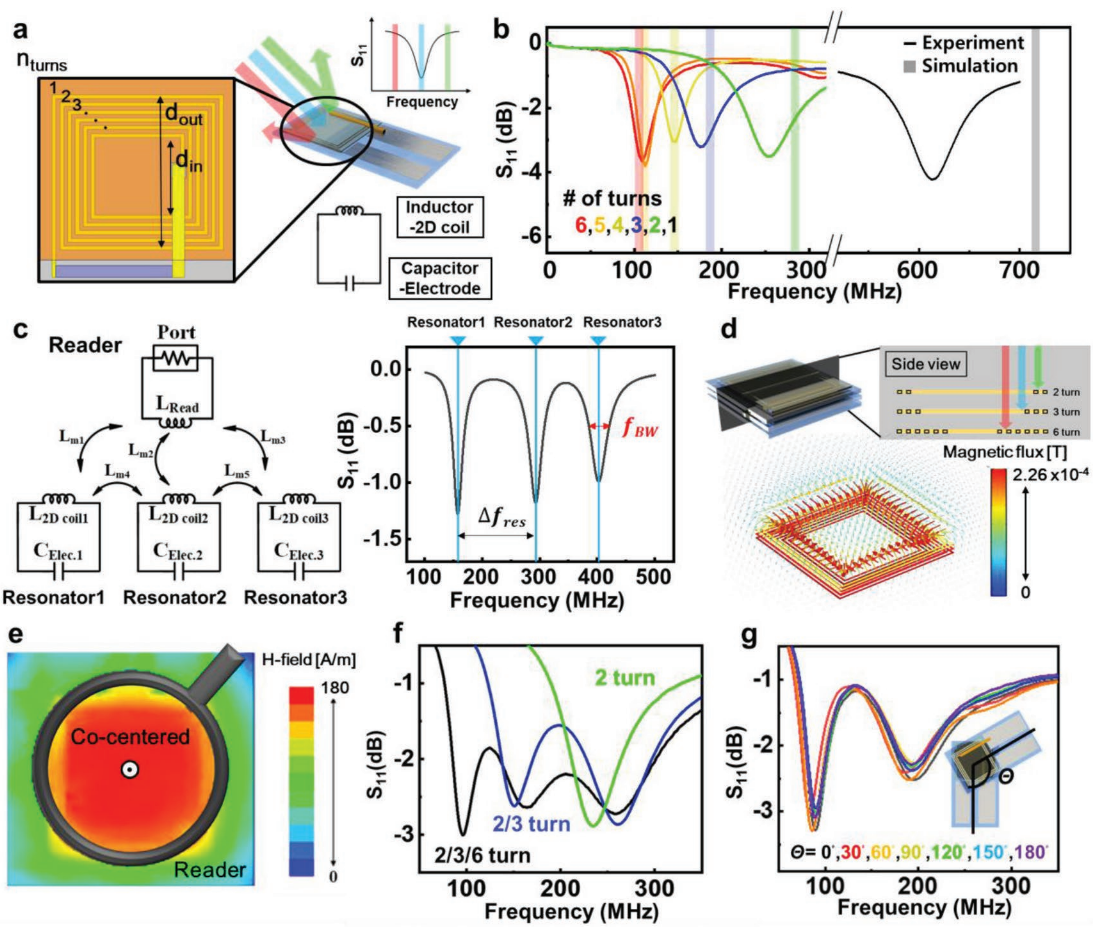

Figure 2. Simulation and experimental results of 2D coil stacking in ascending order. a) 2D coil design, equivalent circuit, and conceptual depiction of the closed LC resonator with a specific resonant frequency. b) Experimental and 3D full-wave EM (3D EM) simulation results of the resonant frequencies of different 2D coils with varying number of turns. c) Circuit simulation of S_{11} spectra of multiple LC resonators with different resonant frequencies. d) Top: 3D EM simulation of the transmission coefficients of the 2D coils in a vertically stacked configuration. Bottom: 3D EM simulation of magnetic flux induction of the stacked 2D coils. e) Top view of magnetic field distribution simulation of the stacked coils in ascending order. f) Experimentally obtained S_{11} spectra of different number of stacked LC resonators in ascending order, each of which had a different number of coil turns. g) Experimentally obtained S_{11} spectra of two stacked LC resonators at different relative rotation angles.

with machine learning to process tactile information. This technology can potentially be used to improve the signal processing capability of various tactile sensors in the future, which is an exciting prospect for prosthetics, robotics, and wearable and implantable electronics.

Figure 1d is a schematic of our wireless pressure sensor. On the right-hand side of a substrate (either glass or poly(lactide-*co*-glycolic acid)), metal-based (Al or Au) 2D coil was patterned in a solution-free manner using vacuum deposition. On the left-hand side, lateral electrodes composed either of Al or Ag nanowires (NWs) were patterned on the glass or poly(dimethylsiloxane) (PDMS). On the 2D coil, the polyimide insulating layer with a via hole was laminated on top; the via hole was aligned to one end of the 2D coil. This end was electrically connected to one of the lateral electrodes with copper (the other end of the 2D coil and the other lateral electrode were already connected during shadow patterning) to form a closed LC resonator. The pressure-sensitive element was made first by microstructuring a PDMS substrate with pyramids, and the surface of the pyramids was chemically grafted with polypyrrole (Ppy), a conductive polymer with a high dielectric constant (>10).[30] Then, this substrate was placed on top of the lateral electrodes with the pyramids facing down (this will be referred to as LC pressure sensor from this point on). A detailed fabrication process and schematics are in Figures S1–S3 in the Supporting Information. Figure 1e is a schematic of vertically stacked 2D coils, through which a reader can simultaneously receive the signals from multiple sensors at a single location, analogous to the junction between primary neurons to a secondary neuron.

Figure 2a depicts the layout of the 2D coil on the left, and an equivalent circuit on the bottom right. As schematically depicted on the top right of Figure 2a, at the resonant frequency (f_{res}) of the closed LC resonator, the electromagnetic (EM) wave is stored, resulting in a sharp decrease in the S_{11} spectrum. The resonant frequency is related to the inductance (L_{2D}) and capacitance (C) of the closed LC resonator by the Equation (1)

$$f_{res} = \frac{1}{2\pi\sqrt{L_{2D}C}} \tag{1}$$

The inductance of the 2D coil is related to the number of turns (n) and the outer (d_{out}) and inner (d_{in}) diameter of the coil by the following equation[31]

$$L_{2D} \propto n^2 \frac{(d_{out} + d_{in})}{2} \tag{2}$$

Considering Equations (1) and (2), the number of turns should be inversely proportional to the resonant frequency. Such a trend has been verified experimentally and using a 3D full-wave EM (3D EM) simulation, as seen in Figure 2b and Figure S4 in the Supporting Information. We have conducted circuit simulation where signals from 3 LC resonators with different resonant frequencies are received by a reader (Figure 2c). As seen in the S_{11} spectrum on the right side of Figure 2c, each LC resonator is assigned a specific frequency. For our experiments, we have used two, three, and six turn 2D coils, which has resonant frequency differences of ≈70 MHz.

Vertically stacking the 2D coils can save valuable space on a device and the signal can be measured simply using standard equipment, which are important features for many different applications such as wearable and implantable electronics. To the best of our knowledge, the vertically stacked closed LC resonator configuration that can read out the signals from multiple sensors has not been previously reported. Figure 2d top is a schematic image of 3D EM simulated transmission coefficients through the 2D coils in a vertically stacked configuration in ascending order (i.e., the 2D coil with a smaller number of turns placed closer to the reader). The transmission coefficients of the two, three, and six turn 2D coils were −3.6 dB (green), −5.7 dB (blue), −7.7 dB (red), respectively, signifying that the EM waves are transmitted to each of the 2D coils with minor shielding from the upper coil.[32] Figure 2d bottom and Figure S5a in the Supporting Information are 3D EM simulation of magnetic flux induction of the stacked 2D coils in ascending and descending (i.e., the 2D coils with a higher number of turns placed closer to the reader) order, respectively. In the ascending order, higher magnetic flux is induced, indicating less interference and shielding effect between the coils. In the descending order, the uppermost coil stores most of the EM wave and hinders its propagation; therefore, S_{11} poles of all of the coils merge into one (Figure S5b, Supporting Information). These results together verify the importance of stacking order of the 2D coils for the differentiation of signal coming from multiple sensors. Figure 2e is a top view 3D EM simulated image of magnetic field distribution of the stacked 2D coils in ascending order, which reveals that the magnetic field is concentrated at the center of the coils. Hence, we were able to measure the combined magnetic field through a commercialized reader coil (HZ-15 RSH400-1, Rohde & Schwarz) without the need for customized measurement equipment.

Figure 2f is the experimentally obtained S_{11} spectra of the different number of stacked LC resonators in ascending order, where each LC resonator had a different number of coil turns (two, three, and six turn). With each addition of LC resonator, the appearance of an additional S_{11} pole was observed. The minor shifting of the resonance frequencies with the addition of S_{11} pole is due to the mutual inductance between the coils (Figure S6, Supporting Information). As mentioned above, the two, three, and six turn 2D coils were chosen to yield resonant frequency difference of ≈70 MHz, which was needed to differentiate the poles without pole-to-pole interference. The resonant frequency difference (Δf_{res}) can be lowered by increasing the Q factor, through which the bandwidths (f_{BW}) of the S_{11} poles can be reduced.[33] Figure 2g is S_{11} spectra of two stacked LC resonators at different relative rotation angles, where no significant difference in the plots was observed. Hence, our system potentially has the freedom to configure the LC pressure sensors in various orientations.

Figure 3a is a side view schematic of the Ppy-coated microstructured PDMS placed on top of the lateral electrodes. The left-most plot of Figure 3c is the experimentally attained S_{11} pole of an LC pressure sensor with three turn coil at various applied pressures up to 10 kPa. The S_{11} pole increased with pressure, suggesting that the stored EM wave decreased with increasing pressure. Meanwhile, there was minimal frequency shifting with applied pressure. The left side of Figure 3b is the 3D full-wave simulation of an LC pressure sensor, where the capacitance between the lateral electrodes was numerically varied as 4 (blue), 7 (green), 10 (orange) pF by modulating the dielectric constant. The simulation also yielded largely increasing S_{11} pole with minimal resonant frequency shifting. In our LC resonator, the stored EM wave is concentrated between the lateral electrodes. When the effective dielectric constant (ε_{eff}) between the electrodes increases, the stored EM wave energy decreases. This leads to an increase of the S_{11} pole value (this mechanism is further explained in Figure S7, Supporting Information).[33] These results suggest that the sensor configuration of Figure 3a functions as a capacitive sensor in our system rather than a piezoresistive sensor. As pressure is applied, the contact area between the Ppy and electrodes increases. The large dielectric constant of Ppy causes an increase in the effective dielectric constant (ε_{eff}) between the lateral electrodes under applied pressure, increasing the capacitance (relation between S_{11} and capacitance is analyzed in Figure S8, Supporting Information). Figure S9, Supporting Information, is a plot of the change in capacitance versus pressure and cycling behavior of our sensor measured using an LCR meter, verifying that our sensor works as a capacitive pressure sensor. The resistance between the electrodes, however, changes trivially with applied pressure since the resistance of Ppy is much larger (≈k Ohms) than that of the coil (tens of Ohms) (i.e., since the electrodes are connected by the coils and Ppy, the two resistances can be modeled as two resistors connected in parallel. In this case, the smaller of the two resistors dominates the overall resistance.)

The right side of Figure 3b is a Smith chart, where the blue, green, and orange circles represent the capacitance between the lateral electrodes of 4, 7, and 10 pF, respectively. The fact that the shortest distance from the origin to a point on the surface of each circle are all in the same direction (i.e., all overlapping in a line) corroborates the small change in resonance frequency at various pressures attained in Figure 3b left and Figure 3c left.[33] Here, we note that the detection of pressure (or any given input) using the change in magnitude has advantages over that of using the change in resonance frequency. First, when signals

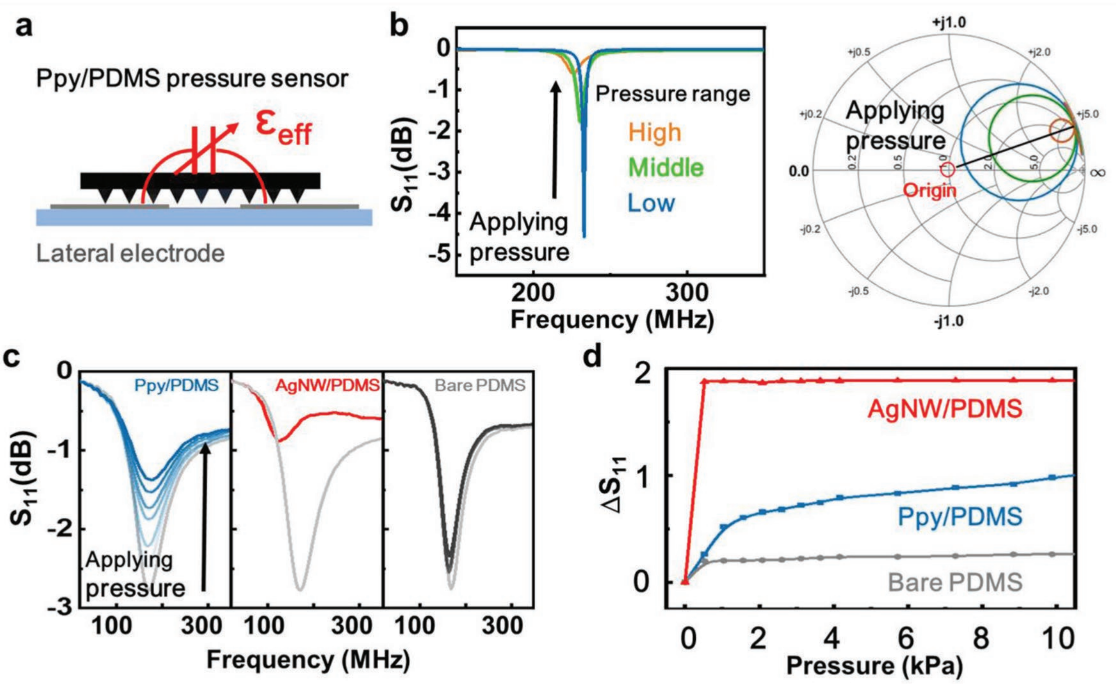

Figure 3. LC pressure sensor characterization and analysis. a) Schematic of the Ppy-coated microstructured PDMS placed on top of the lateral electrodes, working as an effective dielectric constant (ε_{eff}) modulating capacitive pressure sensor. b) 3D EM simulation results of an LC pressure sensor, where the capacitance between the lateral electrodes was numerically varied as 4 (blue), 7 (green), and 10 (orange) pF. Left side is the S_{11} spectra and right side is the Smith chart. c) S_{11} pole of different types of sensors under pressure, up to 10 kPa. d) Change in the magnitude of S_{11} pole as a function of pressure for each type of pressure sensor.

from multiple sensors need to be detected simultaneously, the use of frequency shifting can merge the poles during operation, rendering it difficult to decouple the individual sensor signals. Second, detecting amplitude variation is simple and cost-effective because it does not need additional complex circuit components such as phase locked loop, mixer, and oscillator, which are all required for frequency variation detection systems.[34]

As control experiments, we have coated the PDMS pyramids with Ag NW, and also used PDMS pyramids without any surface coating. As seen in the middle plot of Figure 3c, the Ag NW-based sensor was unable to differentiate pressure levels. This can be attributed to the fact that since Ag NW is a metal with high conductivity, the capacitor is shorted when contact is made with the lateral electrodes, at which the device can no longer function as an LC resonator. On the other hand, when bare PDMS is used, only slight changes in signal were observed since the dielectric constant of PDMS (2.3–2.8) is much lower than that of Ppy (>10).[30] Figure 3d is a plot of change in S_{11} as a function of pressure for the Ag NW-coated, Ppy-coated, and bare PDMS. Evidently, the Ppy-coated PDMS was the most suitable for pressure sensing (0.32 dB kPa^{-1} from 0 to 2 kPa, 0.039 dB kPa^{-1} from 2 to 10 kPa).

Figure 4a–c is S_{11} spectra of three sensor-based WiPPCoP, where 2 kPa of pressure was applied to one sensor at a time. Apparently, the S_{11} pole that corresponds to the pressure sensor being pressed undergoes a dominant change in magnitude. (S_{11} spectra when pressure up to 10 kPa was applied to each sensor are shown in Figure S10, Supporting Information.) Figure 4d–f are S_{11} spectra where 2 kPa of pressure was applied to multiple sensors at a time, which also indicates that the magnitudes change correspondingly. These results verify that WiPPCoP can detect and differentiate the signal from multiple sensors. We note that when the LC pressure sensors are stacked in descending order, all of the S_{11} poles merged; hence, the signals from the sensors could not be differentiated (Figure S11, Supporting Information).

As mentioned above, even with properly stacked coil configuration, there is mutual inductance between the LC pressure sensors. Looking closely at Figure 4a–f, the S_{11} poles corresponding to unpressed sensors undergo a slight change in magnitude. In other words, there is an inevitable crosstalk between the S_{11} poles of each sensor. Hence, when pressure needs to be quantified precisely, and especially for small changes in pressure, the measurement becomes difficult. To overcome this challenge, we have utilized convolutional neural network (CNN)-based machine learning, mimicking the cognitive learning ability of our brain (**Figure 5**a).[35–37] Through cognitive learning, we are able to improve the perception (e.g., quantification, categorization, spatial differentiation) of tactile information and better interact with our surroundings.[38–40] Such an ability is also expected to be an important feature in humanoid applications, as it will enable them to adapt to changes to their surroundings and tasks.[41,42] CNN has connectivity patterns between neurons that resemble the organization of the sensory cortex. Analogously to synaptic strengths and neural receptive fields of the sensory cortex, CNN consists of i) linear operations filtering by a set of weights,[36] ii) a pointwise nonlinear operation, called activation, iii) pooling, a nonlinear

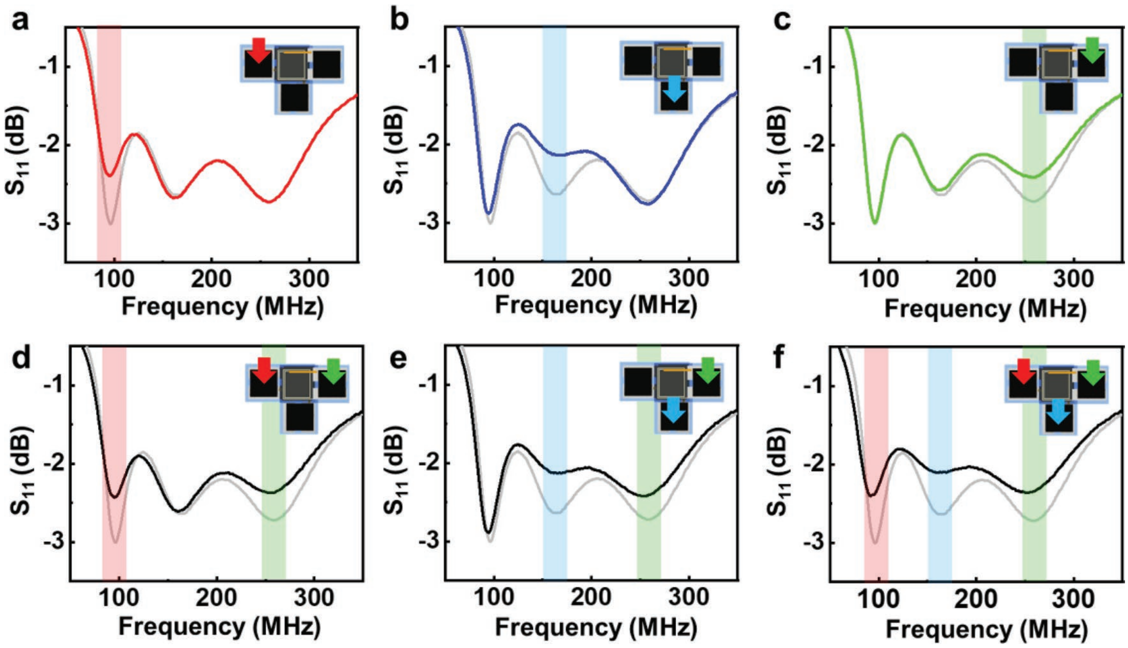

Figure 4. S_{11} spectra of three sensor-based WiPPCoP under the application of 2 kPa of pressure to different sensors. The insets indicate which sensor(s) were pressed.

aggregation operation, and iv) normalization to adjust output values to a reasonable range.[35] The operations within CNN layers can be mapped to cortical areas and organized hierarchically for deep CNN and sensory cortex model, respectively.[36]

The detailed description of CNN machine learning procedure is available in the Experimental Section in the Supporting Information. Briefly stated, a total of 120 data were used, where 100 of them were used as training data and 20 of them were used as test data. Each data was a vector consisting of a column of S_{11} values where pressure levels of varying combinations were applied to the three sensors. Figure 5b is the predicted pressure of one of the test data (representing an average accuracy) after being trained with 100 training data. Evidently, our algorithm was able to predict the pressure levels with

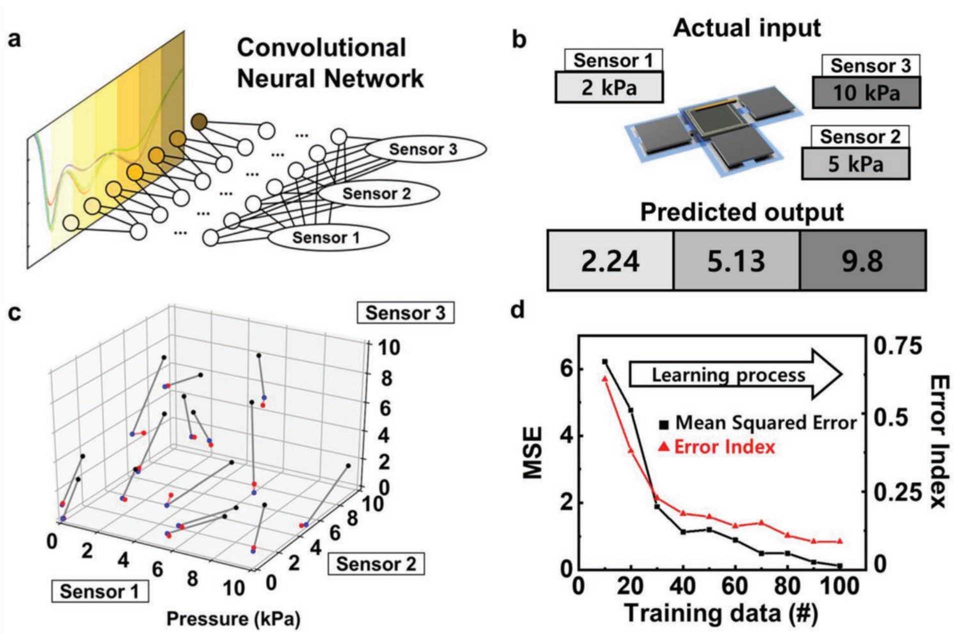

Figure 5. Machine-learning-based pressure signal processing. a) Schematic illustration of CNN. b) Predicted pressures applied to each of the sensors compared to that of actual pressure applied after training with 100 data. c) Visualization plot comparing the actual pressure levels applied to each of the sensors (blue dots) to the predicted pressure levels after training with 10 data (black dots) and 100 data (red dots). d) MSE and error index according to the number of training data.

reasonable accuracy. Figure 5c is a visualization plot comparing the actual pressure levels applied to each of the sensors (blue dots) to the predicted pressure levels after training with 10 data (black dots) and 100 data (red dots). Apparently, the accuracy of the predicted pressure levels improves with more training. Figure 5d is a plot of mean squared error (MSE) and error index after training with varying numbers of data. The error index is defined as

$$\text{Error Index} = \frac{1}{N}\sum \frac{\left|P_{\text{act},i} - P_{\text{pred},i}\right|}{\left|P^*_{\text{act},i}\right|} \tag{3}$$
$$\left(\text{if } \left|P_{\text{act},i}\right| < 1, \left|P^*_{\text{act},i}\right| = 1, \text{ else } P^*_{\text{act},i} = P_{\text{act},i}\right), i \in \{1,2,\ldots N\}$$

where $P_{\text{pred}.i}$ and $P_{\text{act}.i}$ are the expected and actual values of the pressure levels in vector form (i.e., P_{pred} or $P_{\text{act}} = <P_1, P_2, P_3>$, where P_1, P_2, and P_3 are pressure levels applied to each of the three sensors), $P_{\text{act},i}$* is a normalization factor to generate absolute percentage error, and N is the number of samples. Both the MSE and error index decrease with increasing training data. The MSE and error index after training with 100 data were 0.12 and 0.09, respectively, which are sufficiently low to suggest a high predictive accuracy of our algorithm. When each sensor was individually calibrated (i.e., signal pattern was attained by applying different levels of pressure to one sensor at a time, and the resulting data were used as input training data), the error index came out to be 0.24. Hence, the use of signal pattern coming from the simultaneous application of pressure to the three sensors as the training data in machine learning was important for accurate prediction of pressure levels. We have also conducted machine learning on five sensor (2D coils with one, two, three, four, and six turn)-based WiPPCoP, which also exhibited decreasing MSE and error index with increasing training. After training with 200 data, MSE and error index were 0.27 and 0.12, respectively (Figure S12, Supporting Information).

Real-time monitoring of pressure levels is essential for many tactile sensing applications. WiPPCoP's ability to simultaneously receive and differentiate pressure signals from multiple sensors was utilized to conduct real-time monitoring of pressures at different locations, as depicted in **Figure 6**a (see the Experimental Section in the Supporting Information for details). We have also made the LC pressure sensor flexible and placed it on a human finger to detect pressure (Figure 6b,c). All of the components being passive made it relatively easy to render it flexible (see Figure S13 in the Supporting Information for details of the fabrication process, and Figure S14 in the Supporting Information for the acquired signal under bending of the sensing region). When the distance between the reader and the stacked coils was varied, the magnitudes of the S_{11} poles changed in similar proportions (Figure S15, Supporting Information); thus, by calibrating the signal at different distances, the pressure levels can in principle be analyzed.[43] These are all important features in wearable and implantable electronic applications.

Herein, inspired from the human somatosensory system, we introduced WiPPCoP, where pressure inputs from multiple sensors were received in parallel and combined into one output signal at a single location using stacked 2D coil architecture. For minimal interference between the coils, the coil with smaller number of turns was placed closer to the reader. The stacked architecture saves valuable space on a given device, and the signal can be processed in a facile manner using a standard reader. The pressure sensor functioned as a capacitive sensor, where the applied pressure increased the effective dielectric constant between the lateral electrodes. By varying the design of 2D coil geometry, each pressure sensor was assigned a specific frequency on the S_{11} spectrum, and the applied pressure changes the magnitude of the S_{11} poles with minimal frequency shifting. This is an important property for multi-sensor signal processing, as the signal from each sensor can easily be identified. Finally, CNN-based machine learning was implemented to predict the pressure values from unforeseen S_{11} spectra. The accuracy of prediction was relatively high with MSE of 0.12. Although we demonstrated WiPPCoP with three or five sensors, the number of sensors can be expanded by 1) broadening the operating frequency via fabricating smaller or larger 2D coils, and 2) by reducing the difference between the resonant frequencies of each sensor by decreasing the bandwidth of the poles (i.e., the Q factor is related to the bandwidth). However, as the number of sensors continue to increase to a large number, challenges are expected to arise. For instance, with an increasing number of LC pressure sensors, the combined signal pattern will be difficult to process due to the complicated mutual inductance between the stacked coils. It will require more advanced machine learning algorithms and a large amount of training data. Another issue of our system is the complexity of the monolithic integration of a large number of sensors since many layers need to be patterned and aligned vertically. Further study and development of novel fabrication process are needed to address this issue.

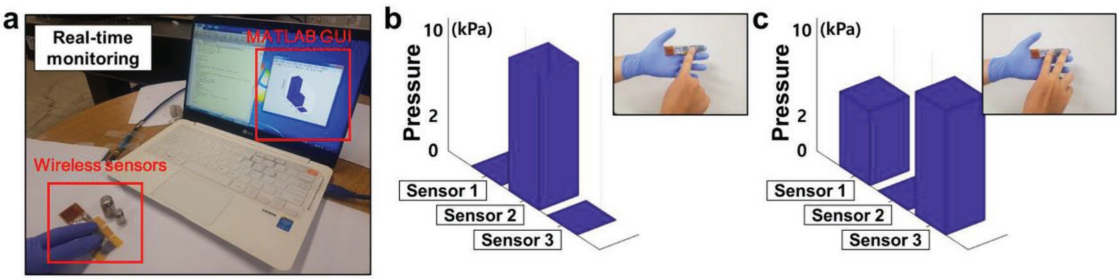

Figure 6. Real-time monitoring of pressure. a) Photograph image of real-time monitoring. b,c) Real-time monitoring of pressure using a flexible WiPPCoP placed on an index finger.

In summary, WiPPCoP can eliminate complex off-chip wiring, acquire and process signal coming from multiple sensors in parallel, and has the potential to consistently improve its accuracy during its operation and adapt to new environments through the use of machine learning.[44,45] We project that WiPPCoP will be an important groundwork for the rapid advancement of tactile sensing electronic skin for practical applications in the near future.

Experimental Section

Experimental Section is available in the Supporting Information.

Supporting Information

Supporting Information is available from the Wiley Online Library or from the author.

Acknowledgements

G.-H.L. and J.-K.P. contributed equally to this work. This work was supported by National Research Foundation of Korea (NRF) grant funded by the Korea government (MSIT) (No. 2019R1C1C1006928), Institute for Information & communications Technology Promotion (IITP) grant funded by the Korea government (MSIT) (No. 2017-0-00048) and a research which has been conducted as part of the KAIST-funded Global Singularity Research Program for 2019.

Conflict of Interest

The authors declare no conflict of interest.

Keywords

electronic skin, *LC* passive resonators, machine learning, parallel signal processing, pressure sensors

Received: September 24, 2019
Revised: November 22, 2019
Published online: December 16, 2019

[1] M. L. Hammock, A. Chortos, B. C. K. Tee, J. B. H. Tok, Z. A. Bao, *Adv. Mater.* **2013**, *25*, 5997.
[2] T. T. Yang, D. Xie, Z. H. Li, H. W. Zhu, *Mater. Sci. Eng., R* **2017**, *115*, 1.
[3] J. C. Yang, J. Mun, S. Y. Kwon, S. J. Park, Z. A. Bao, S. Park, *Adv. Mater.* **2019**, *31*, 1904765.
[4] M. Ha, S. Lim, H. Ko, *J. Mater. Chem. B* **2018**, *6*, 4043.
[5] A. Chortos, J. Liu, Z. A. Bao, *Nat. Mater.* **2016**, *15*, 937.
[6] C. Jeong, J. S. Lee, B. Park, C. S. Hong, J. U. Kim, T. I. Kim, *Adv. Mater.* **2019**, *31*, 1902689.
[7] Z. G. Qiu, Y. B. Wan, W. H. Zhou, J. Y. Yang, J. L. Yang, J. Huang, J. M. Zhang, Q. X. Liu, S. Y. Huang, N. N. Bai, Z. G. Wu, W. Hong, H. Wang, C. F. Guo, *Adv. Funct. Mater.* **2018**, *28*, 1802343.
[8] H. H. Chou, A. Nguyen, A. Chortos, J. W. F. To, C. Lu, J. G. Mei, T. Kurosawa, W. G. Bae, J. B. H. Tok, Z. A. Bao, *Nat. Commun.* **2015**, *6*, 6616.
[9] Y. Lee, J. Park, S. Cho, Y. E. Shin, H. Lee, J. Kim, J. Myoung, S. Cho, S. Kang, C. Baig, H. Ko, *ACS Nano* **2018**, *12*, 4045.
[10] J. C. Yang, J. O. Kim, J. Oh, S. Y. Kwon, J. Y. Sim, D. W. Kim, H. B. Choi, S. Park, *ACS Appl. Mater. Interfaces* **2019**, *11*, 19472.
[11] R. S. Dahiya, G. Metta, M. Valle, G. Sandini, *IEEE Trans. Rob.* **2009**, *26*, 1.
[12] C. M. Boutry, M. Negre, M. Jorda, O. Vardoulis, A. Chortos, O. Khatib, Z. N. Bao, *Sci. Rob.* **2018**, *3*, eaau6914.
[13] Q. L. Hua, J. L. Sun, H. T. Liu, R. R. Bao, R. M. Yu, J. Y. Zhai, C. F. Pan, Z. L. Wang, *Nat. Commun.* **2018**, *9*, 244.
[14] B. W. Zhu, H. Wang, Y. Q. Liu, D. P. Qi, Z. Y. Liu, H. Wang, J. C. Yu, M. Sherburne, Z. H. Wang, X. D. Chen, *Adv. Mater.* **2016**, *28*, 1559.
[15] J. H. Yoon, Z. R. Wang, K. M. Kim, H. Q. Wu, V. Ravichandran, Q. F. Xia, C. S. Hwang, J. J. Yang, *Nat. Commun.* **2018**, *9*, 417.
[16] Y. Kim, A. Chortos, W. T. Xu, Y. X. Liu, J. Y. Oh, D. Son, J. Kang, A. M. Foudeh, C. X. Zhu, Y. Lee, S. M. Niu, J. Liu, R. Pfattner, Z. N. Bao, T. W. Lee, *Science* **2018**, *360*, 998.
[17] C. J. Wan, G. Chen, Y. M. Fu, M. Wang, N. Matsuhisa, S. W. Pan, L. Pan, H. Yang, Q. Wan, L. Q. Zhu, X. D. Chen, *Adv. Mater.* **2018**, *30*, 1801291.
[18] D. U. Silverthorn, *Human Physiology: An Integrated Approach*, Pearson, London, UK **2015**.
[19] D. Purves, G. J. Augustine, D. Fitzpatrick, W. C. Hall, A. S. LaMantia, J. O. McNamara, L. E. White, *Neuroscience*, Sinauer, Sunderland, MA, USA **2008**.
[20] E. A. Lumpkin, M. J. Caterina, *Nature* **2007**, *445*, 858.
[21] C. D. Gilbert, T. N. Wiesel, *Nature* **1992**, *356*, 150.
[22] R. H. Hamilton, A. Pascual-Leone, *Trends Cognit. Sci.* **1998**, *2*, 168.
[23] A. M. Fernandes, P. B. Albuquerque, *Cognit. Process.* **2012**, *13*, 285.
[24] Y. C. Pei, S. S. Hsiao, J. C. Craig, S. J. Bensmaia, *Neuron* **2011**, *69*, 536.
[25] C. M. Klingner, S. Brodoehl, R. Huonker, T. Gotz, L. Baumann, O. W. Witte, *NeuroImage* **2015**, *118*, 193.
[26] C. J. Wan, P. Q. Cai, M. Wang, Y. Qian, W. Huang, X. D. Chen, *Adv. Mater.* https://doi.org/10.1002/adma.201902434.
[27] L. Y. Chen, B. C. K. Tee, A. L. Chortos, G. Schwartz, V. Tse, D. J. Lipomi, H. S. P. Wong, M. V. McConnell, Z. A. Bao, *Nat. Commun.* **2014**, *5*, 5028.
[28] J. Kim, M. Kim, M. S. Lee, K. Kim, S. Ji, Y. T. Kim, J. Park, K. Na, K. H. Bae, H. K. Kim, F. Bien, C. Y. Lee, J. U. Park, *Nat. Commun.* **2017**, *8*, 14997.
[29] A. Palmroth, T. Salpavaara, J. Lekkala, M. Kellomaki, *Adv. Mater. Technol.* **2019**, *4*, 1900428.
[30] P. Du, X. Lin, X. Zhang, *J. Phys. D: Appl. Phys.* **2013**, *46*, 195303.
[31] S. S. Mohan, M. D. Hershenson, S. P. Boyd, T. H. Lee, *IEEE J. Solid-State Circuits* **1999**, *34*, 1419.
[32] S. Cheon, Y. H. Kim, S. Y. Kang, M. L. Lee, J. M. Lee, T. Zyung, *IEEE Trans. Ind. Electron.* **2011**, *58*, 2906.
[33] D. M. Pozar, *Microwave Engineering*, John Wiley & Sons, Hoboken, NJ **2009**.
[34] R. E. Ziemer, W. H. Tranter, *Principles of Communications*, John Wiley & Sons, Hoboken, NJ, USA **2014**.
[35] Y. Bengio, *Learning Deep Architectures for AI*, Now Publishers, Hanover, MA, USA **2009**.
[36] D. L. K. Yamins, J. J. DiCarlo, *Nat. Neurosci.* **2016**, *19*, 356.
[37] M. Carandini, D. J. Heeger, *Nat. Rev. Neurosci.* **2012**, *13*, 51.
[38] W. C. Abraham, M. F. Bear, *Trends Neurosci.* **1996**, *19*, 126.
[39] P. Ragert, A. Schmidt, E. Altenmuller, H. R. Dinse, *Eur. J. Neurosci.* **2004**, *19*, 473.

[40] D. T. Blake, M. A. Heiser, M. Caywood, M. M. Merzenich, *Neuron* **2006**, *52*, 371.
[41] M. Asada, K. F. MacDorman, H. Ishiguro, Y. Kuniyoshi, *Rob. Auton. Syst.* **2001**, *37*, 185.
[42] D. Y. Little, F. T. Sommer, *Front. Neural Circuits* **2013**, *7*, 37.
[43] S. M. Niu, N. Matsuhisa, L. Beker, J. X. Li, S. H. Wang, J. C. Wang, Y. W. Jiang, X. Z. Yan, Y. J. Yun, W. Burnetts, A. S. Y. Poon, J. B. H. Tok, X. D. Chen, Z. N. Bao, *Nat. Electron.* **2019**, *2*, 361.
[44] G. I. Parisi, R. Kemker, J. L. Part, C. Kanan, S. Wermter, *Neural Networks* **2019**, *113*, 54.
[45] Y. Ganin, E. Ustinova, H. Ajakan, P. Germain, H. Larochelle, F. Laviolette, M. Marchand, V. Lempitsky, *J. Mach. Learn. Res.* **2016**, *17*, 2096.